

ON THE OCCURRENCE OF SYSTEMATIC ERRORS IN CROSS-CORRELATION BASED MEASUREMENTS FOR AERODYNAMICS

F. Blumrich

German Aerospace Center, Linder Hoehe, 51147 Cologne, Germany

Keywords: *sub-pixel, displacement estimation, cross-correlation, particle image velocimetry, least squares estimation*

Abstract

The scope of this paper is the investigation of sub-pixel displacement estimation in cross-correlation based measurement techniques used in aerodynamics. We will show, that a systematic error will occur when using one-dimensional sub-pixel displacement estimation algorithms to decompose elliptically shaped correlation peaks. First, an analytical description of this error will be derived and it will be shown, that it can lead to a systematic influence of more than one pixel. Additionally, a general linear two-dimensional Gaussian algorithm based on least squares estimation will be presented to allow for sub-pixel displacement estimation of elliptically shaped correlation peaks without any significant bias error. The performance of the here presented algorithms for sub-pixel displacement estimation, as well as algorithms provided by commercial software packages, will be tested with artificial image pairs of random dot patterns.

1 Introduction

For over 25 years, digital image correlation (DIC) techniques have been used in scientific research and developments. In the early 1980s, a group from the University of Stuttgart [1, 2, 3] used DIC in photogrammetry and remote sensing to match homologous image areas with an accuracy of up to 0.01 pixel. This enables DIC to be a powerful tool for several photogrammetric applica-

tions like automatic tie point transfer, digital elevation models, and relative orientation. The basic approach of this group is to correlate local image areas two-dimensionally [2]. Instead of the most commonly used procedure of maximization of the cross-correlation coefficient, they used a transformation which minimizes the grey value differences in a least squares sense [3]. This approach as well as the work of A. Grün (see [4]) is also referred to as least squares matching (LSM). At the same time, researchers from the University of South Carolina [5] were the first to use two-dimensional DIC for the evaluation of deformation measurements. Therefore, they applied a random speckle pattern to the surface and recorded the pattern in a reference and a deformed state of the object. The cross-correlation of this image pair yields a measure of surface displacement. Using a large number of different subsets for cross-correlation, full-field displacement data can be obtained for the image pair.

In the last few years, the DIC method has been extended to three-dimensional shape and deformation measurements by means of a stereo camera setup. Using at least two synchronized high-speed cameras, it is possible to measure highly dynamic objects [6]. Besides DIC, many other optical correlation-based measurement techniques like particle image velocimetry (PIV) [7, 8, 9, 10], projected pattern correlation (PROPAC) [11, 12], and background oriented Schlieren (BOS) [13, 14] are used in sci-

entific research. All these techniques have one thing in common: their accuracy is limited by reconstruction errors due to geometric calibration of the system and by errors caused by the correlation algorithm itself (see [6]). The high sub-pixel accuracy of the correlation algorithm can be achieved by means of sub-pixel displacement estimation algorithms [15]. According to [10] we can expect the sub-pixel accuracy of the correlation of a 32×32 pixel sample from an 8 bit image to be in the order of 0.1 to 0.05 pixel. Uncertainties in digital image correlation techniques can be due to random errors, e.g. image noise, or due to bias errors of the correlation procedure and the sub-pixel displacement estimation algorithm (see [16]).

Nowadays, there are a lot of different sub-pixel displacement estimation algorithms available. Commonly used algorithms consist of two one-dimensional fits through the highest value and its neighbors in both horizontal and vertical direction. These algorithms are normally referred to as three-point operators [10], if only the direct neighbor values are used. Typically curve fitting with a Gaussian [7, 8, 17] or parabolic [17, 18] function is used. Gradient-based algorithms, like suggested by [19, 20], or algorithms based on ideal interpolation [21, 22] (also referred to as Whittaker reconstruction) are more general because no a priori information about the shape of the peak is needed. Alexander and Ng (see [23]) introduced the centroid operator for the detection of light stripe location in active triangulation. This algorithm can be used in a one- or two-dimensional sense and is implemented very easily. Two-dimensional Gaussian curve fitting algorithms are first described by [24] for applications in astronomy and later on by [25] for aerodynamic applications. In [26], a two-dimensional iterative Levenberg-Marquardt fit using correlation values weighted according to the Fisher transform is presented. Some work has been done comparing different sub-pixel displacement estimation algorithms (see [15, 17, 18, 20, 27]) and on the impact of systematic errors in the correlation and peak detection process (see [16, 28]).

As a result of the oblique projection of circu-

lar dots in the PROPAC technique and also in the image corners of standard random dot patterns imaging techniques, elliptically shaped correlation peaks can be obtained. Additionally, state-of-the-art PIV evaluation techniques like image deformation methods [9] will lead to elliptically shaped correlation peaks even if the particles in the undeformed images are circular. In that case, the one-dimensional algorithms will introduce a bias error for the estimated displacement. The scope of this work will be the investigation of the introduced bias error in sub-pixel displacement estimation algorithms using them for elliptically shaped correlation peaks.

The principles of different algorithms for sub-pixel displacement estimation are presented in section 2. Additionally, a general linear two-dimensional Gaussian algorithm for sub-pixel displacement estimation is introduced. In section 3, an analytical equation for the bias error due to elliptically shaped correlation peaks is derived. A numerical experiment with different sub-pixel algorithms on artificial data is carried out in section 4 and the results of the simulation are compared with the analytical solution.

2 Sub-pixel displacement estimation

With the two intensity images I_A and I_B , the two-dimensional discrete cross-correlation function $R_{r,c}$ can be derived as

$$R_{r,c} = \frac{1}{N^2} \sum_{i=1}^N \sum_{j=1}^N (I_A[i, j] - \bar{I}_A) \cdot (I_B[i+r, j+c] - \bar{I}_B), \quad (1)$$

where \bar{I} (with respect to A and B) is the mean intensity image. Initially, the cross-correlation peak position at integer level is found at

$$R_{0,0} = \max(R_{r,c}) \quad (2)$$

as the maximum of the array of cross-correlation values.

A distant point source will appear as an Airy pattern in the image plane due to the circular aperture. This Airy intensity distribution can be

approximated by a Gaussian function. The cross-correlation between two Gaussian intensity distributions will result in a Gaussian intensity distribution. Therefore, the sub-pixel displacement estimation algorithms based on a Gaussian distribution are used very often.

2.1 One-dimensional sub-pixel displacement estimation algorithms

2.1.1 Gaussian interpolation

Assuming that the correlation peak of the displacement between the images I_A and I_B has an approximate one-dimensionally Gaussian shape in both the horizontal and vertical cross-section,

$$\delta = \frac{\ln R_{-1} - \ln R_{+1}}{2(\ln R_{-1} + \ln R_{+1} - 2\ln R_0)} \quad (3)$$

can be used as an estimator of the fractional displacement in both directions using 3 points (see [7, 8]).

2.1.2 Blais-Rioux method

The peak detector developed by Blais and Rioux (see [19]) was originally intended for real-time applications in low-cost laser triangulation sensors. Therefore Finite Impulse Response (FIR) filters were used due to their easy implementation in integrated circuits (ICs). The signal is first averaged and differentiated numerically by

$$BR(s) = -R_{-2} - R_{-1} + R_1 + R_2. \quad (4)$$

It should be mentioned that the filter in Eq. (4) uses 5 values, but is normally referred to as Blais-Rioux operator 4th order in the literature. It is also possible to use different filter lengths combining numerical averaging and differentiating. The resulting signal $BR(s)$ has a zero-crossing where R_i has its maximum. Therefore, the sub-pixel peak position can be calculated using linear interpolation

$$\delta = \frac{BR(s_0)}{BR(s_0) - BR(s_0 + 1)}, \quad (5)$$

where $BR(s_0) \geq 0$ and $BR(s_0 + 1) < 0$ is satisfied. The Blais-Rioux method does not use a priori information about the peak shape like the Gaussian

interpolation. It was demonstrated by different studies [18, 19, 20], that the Blais-Rioux method is very robust against noisy data because of its bandpass character.

Even if the intensity distribution in front of the CCD is Gaussian shaped, the resulting signal is not exactly Gaussian due to the limited fill factor of CCDs and the pixel integration. Therefore there may be some advantages in the use of non-Gaussian algorithms for sub-pixel displacement estimation.

2.2 Two-dimensional sub-pixel displacement estimation algorithms

2.2.1 Gaussian regression

A general two-dimensional elliptical Gaussian function described with six parameters (see [24]) is given by

$$G(x, y) = A \exp \left[-\frac{(x - x_e)^2}{2\sigma_x^2} - \frac{\beta(x - x_e)(y - y_e)}{\sigma_x \sigma_y} - \frac{(y - y_e)^2}{2\sigma_y^2} \right], \quad (6)$$

where (x_e, y_e) is the center of the ellipse, σ_x and σ_y are the 1σ -lengths of the axes, A is the peak amplitude and β contains the information about the ellipse rotation with respect to the coordinate axes (x, y) . To estimate the six parameters of the ellipse, Eq. (6) is first rewritten as follows

$$\ln\{G(x, y)\} = ax^2 + by^2 + cxy + dx + ey + f, \quad (7)$$

but can also be expressed as a linear system of equations

$$\mathbf{y} = \mathbf{Ax}, \quad (8)$$

with the coefficient matrix \mathbf{A}

$$\mathbf{A} = \begin{bmatrix} x_1^2 & y_1^2 & x_1 y_1 & x_1 & y_1 & 1 \\ \vdots & \vdots & \vdots & \vdots & \vdots & \vdots \\ x_1^2 & y_n^2 & x_1 y_n & x_1 & y_n & 1 \\ x_2^2 & y_1^2 & x_2 y_1 & x_2 & y_1 & 1 \\ \vdots & \vdots & \vdots & \vdots & \vdots & \vdots \\ x_2^2 & y_n^2 & x_2 y_n & x_2 & y_n & 1 \\ \vdots & \vdots & \vdots & \vdots & \vdots & \vdots \\ x_m^2 & y_1^2 & x_m y_1 & x_m & y_1 & 1 \\ \vdots & \vdots & \vdots & \vdots & \vdots & \vdots \\ x_m^2 & y_n^2 & x_m y_n & x_m & y_n & 1 \end{bmatrix}, \quad (9)$$

the observation vector \mathbf{y}

$$\mathbf{y} = \begin{bmatrix} \ln\{G(x_1, y_1)\} \\ \vdots \\ \ln\{G(x_1, y_n)\} \\ \ln\{G(x_2, y_1)\} \\ \vdots \\ \ln\{G(x_2, y_n)\} \\ \vdots \\ \ln\{G(x_m, y_1)\} \\ \vdots \\ \ln\{G(x_m, y_n)\} \end{bmatrix} \quad (10)$$

and the vector of unknowns \mathbf{x}

$$\mathbf{x} = \begin{bmatrix} a \\ b \\ c \\ d \\ e \\ f \end{bmatrix}. \quad (11)$$

According to the Gauss-Markov theorem and assuming zero mean, uncorrelated errors which have equal variances, the best linear unbiased estimator (BLUE) of Eq. (8) is

$$\hat{\mathbf{x}} = (\mathbf{A}^T \mathbf{A})^{-1} \mathbf{A}^T \mathbf{y}. \quad (12)$$

The center position of the ellipse can be derived from Eqs. (7) to (12) as

$$x_e = \frac{ce - 2bd}{4ab - c^2}, \quad (13)$$

$$y_e = \frac{cd - 2ae}{4ab - c^2}. \quad (14)$$

Nobach and Honkanen presented an explicit solution to the Gaussian regression for the special case of a fit area strictly limited to 3×3 or 9 values respectively (see [25]). The general solution of the problem introduced here is equivalent to the explicit one of [25], but can be further used for more general fit areas. Moreover there is no limitation to quadratic areas. The only requirement is that at least six observations must be used; otherwise Eq. (12) is under-determined. Compared to the iterative non-linear approach from [26]), this solution can be implemented very fast and effectively.

3 Bias errors using one-dimensional algorithms for sub-pixel displacement estimation

The contour lines of a continuous two-dimensional Gaussian function according to Eq. (6) in a local coordinate system (x, y) centered at the highest value of the discrete cross-correlation function, can be described with the following parameters: The sub-pixel peak position (x_e, y_e) with $|x_e| \leq 0.5$ and $|y_e| \leq 0.5$, the rotation angle α and the numerical eccentricity

$$\varepsilon = \frac{\sqrt{u^2 - v^2}}{u}, \quad (15)$$

where u and v denote the length of the semi-major axis and the semi-minor axis respectively. Using one-dimensional algorithms for sub-pixel displacement estimation means searching for the sub-pixel position of the maximum along the x and y coordinate axis respectively. As clearly seen in Fig. 1, this maximum position in each direction is given by the point of tangency between the coordinate axis and the corresponding contour line. Thus, one-dimensional algorithms will result in the biased peak position (x_p, y_p) , with

$$x_p = x_e - \frac{y_e \varepsilon^2 \sin \alpha \cos \alpha}{1 - \varepsilon^2 \cos^2 \alpha}, \quad (16)$$

$$y_p = y_e - \frac{x_e \varepsilon^2 \sin \alpha \cos \alpha}{1 - \varepsilon^2 \sin^2 \alpha} \quad (17)$$

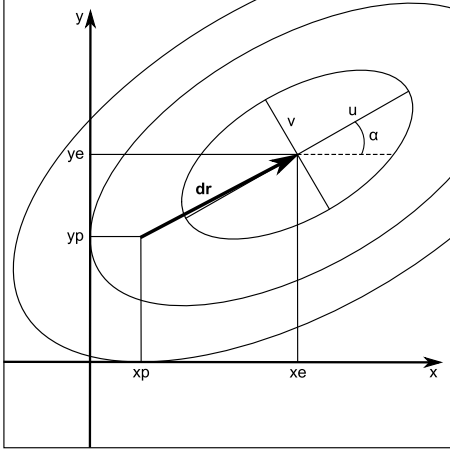


Fig. 1 Graphical illustration of the bias error using a one-dimensional sub-pixel displacement estimation algorithm in the case of an elliptically shaped correlation function.

or in the bias vector, the position difference between (x_e, y_e) and (x_p, y_p)

$$\mathbf{d}_r = -\varepsilon^2 \sin \alpha \cos \alpha \begin{bmatrix} \frac{y_e}{1 - \varepsilon^2 \cos^2 \alpha} \\ \frac{x_e}{1 - \varepsilon^2 \sin^2 \alpha} \end{bmatrix} \quad (18)$$

and its absolute value

$$\|\mathbf{d}_r\| = \varepsilon^2 \sin \alpha \cos \alpha \cdot \sqrt{\left(\frac{y_e}{1 - \varepsilon^2 \cos^2 \alpha}\right)^2 + \left(\frac{x_e}{1 - \varepsilon^2 \sin^2 \alpha}\right)^2} \quad (19)$$

respectively.

Fig. 2, 3 and 4 illustrate the bias error for different types of ellipses graphically. Note that for a fixed center position (x_e, y_e) and eccentricity ε the bias error varies for different rotation angles α . Additionally, the bias error increases for higher eccentricities and center positions further away from the coordinate origin. The bias error disappears for rotation angles $\alpha = 0$ (this means axially-oriented ellipses) or $\varepsilon = 0$ (which corresponds to a circle). The variation of the absolute value of the bias error vector $\|\mathbf{d}_r\|$ with varying rotation angles α is shown in Fig. 5 for difference types of ellipses. Again, it can be noticed that the error increases along with higher eccentricities. In some cases, the error can exceed values of one pixel.

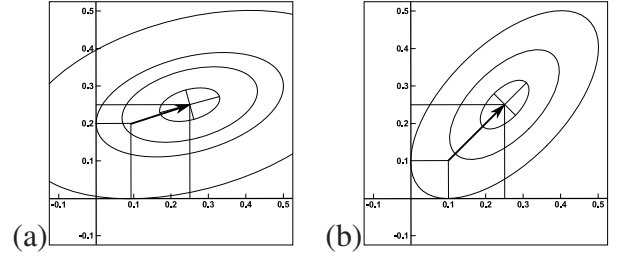


Fig. 2 Example of the bias error using a one-dimensional sub-pixel displacement estimation algorithm. The ellipse center is at $x_e = y_e = 0.25$ pixel, the eccentricity is $\varepsilon = 0.866$ ($u = 2v$) and the rotation angle: (a) $\alpha = 15^\circ$, (b) $\alpha = 45^\circ$.

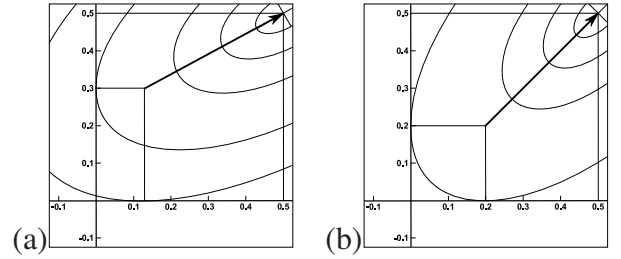


Fig. 3 Example of the bias error using a one-dimensional sub-pixel displacement estimation algorithm. The ellipse center is at $x_e = y_e = 0.5$ pixel, the eccentricity is $\varepsilon = 0.866$ ($u = 2v$) and the rotation angle: (a) $\alpha = 30^\circ$, (b) $\alpha = 45^\circ$.

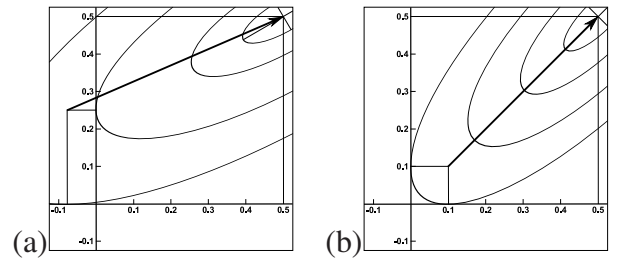


Fig. 4 Example of the bias error using a one-dimensional sub-pixel displacement estimation algorithm. The ellipse center is at $x_e = y_e = 0.5$ pixel, the eccentricity is $\varepsilon = 0.9428$ ($u = 3v$) and the rotation angle: (a) $\alpha = 30^\circ$, (b) $\alpha = 45^\circ$.

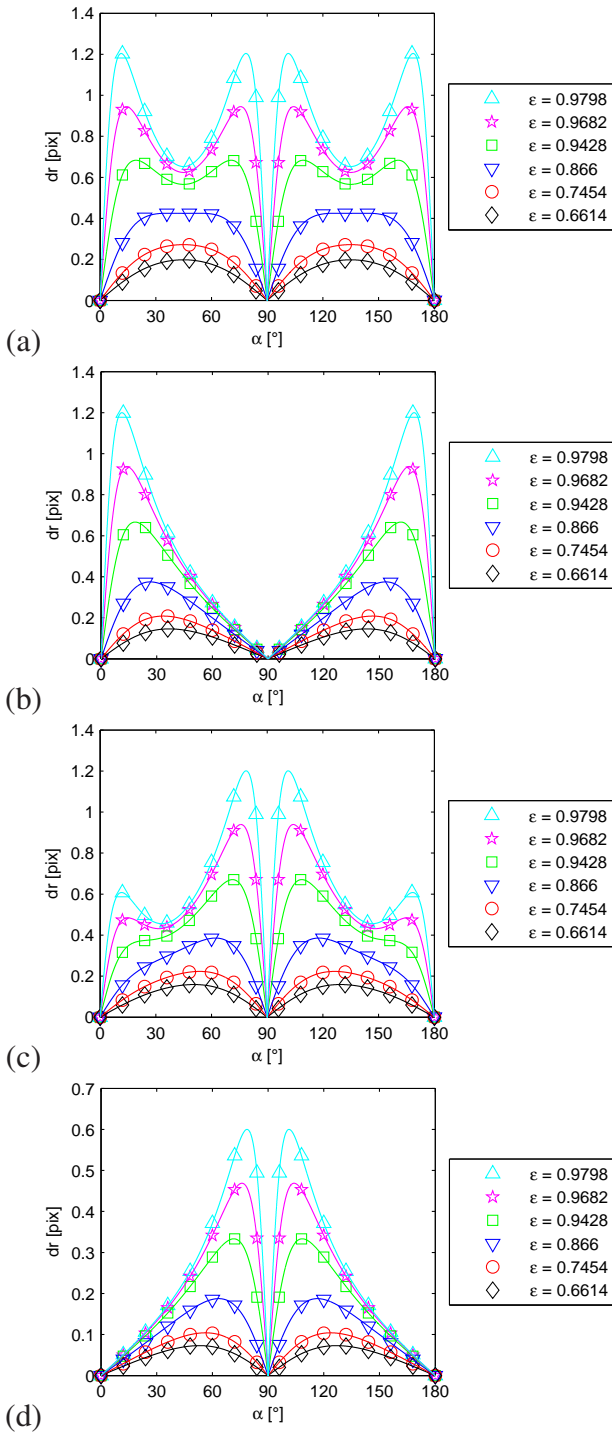


Fig. 5 Absolute value of the bias error (in pixel) using a one-dimensional sub-pixel displacement estimation algorithm for different rotation angles and eccentricities. Ellipse center (in pixel) at: (a) $x_e = 0.5, y_e = 0.5$, (b) $x_e = 0.0, y_e = 0.5$, (c) $x_e = 0.5, y_e = 0.25$, (d) $x_e = 0.25, y_e = 0.0$.

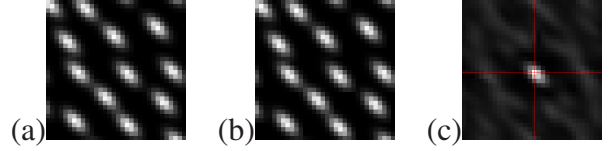


Fig. 6 Correlation procedure with a simulated image pair of known displacement: (a) artificial image with random dot pattern, (b) artificial image with random dot pattern displaced by $(\Delta x, \Delta y)$, (c) resulting cross-correlation function.

4 Verification by numerical experiment

To verify the results so far, synthetic images with random dot patterns were generated. This was done using a Gaussian intensity distribution according to Eq. (6) for every single particle. So it is possible to generate image pairs with known constant sub-pixel displacement (see Fig. 6(a)–(b)) and calculate the resulting cross-correlation function (see Fig. 6(c)) according to Eq. (1). Note that this discrete correlation function is not exactly Gaussian shaped due to the image sampling at discrete pixel positions.

A simulation with elliptically shaped particle images over different displacements $(\Delta x, \Delta y)$, reaching from -0.5 to $+0.5$ pixel in each direction was carried out. Using a step size of 0.05 pixel, this results in 441 different displacement vectors. For every displacement vector, 37 different rotation angles α (reaching from 0° to 90° with a step size of 2.5°) and 121 different sub-pixel center positions of the particles were used. For every combination of displacement vectors, rotation angles and center positions, the cross-correlation of the synthetic image pair was calculated and evaluated with the sub-pixel displacement estimation algorithms described in section 2. Thus, the error of the sub-pixel displacement estimation is

$$\|\mathbf{d}_r^{sim}\| = \sqrt{(\Delta x - x_p)^2 + (\Delta y - y_p)^2}, \quad (20)$$

where $(\Delta x, \Delta y)$ is the known displacement and (x_p, y_p) the calculated displacement of the sub-pixel displacement estimation algorithm. Using one-dimensional sub-pixel displacement es-

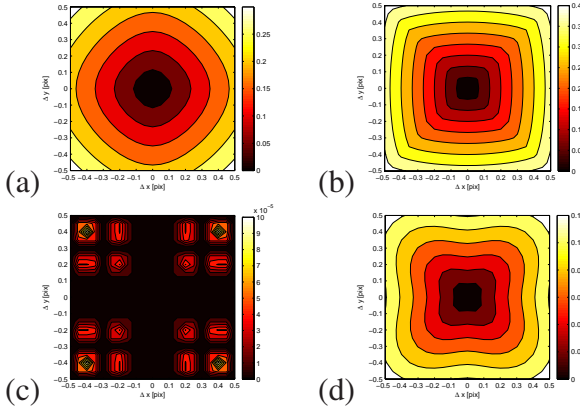


Fig. 7 Sub-pixel displacement estimation error using the one-dimensional Gaussian algorithm: (a) mean, (b) maximum, (c) minimum, (d) standard deviation.

estimation algorithms and assuming that the cross-correlation itself has no systematic error, this error should be the same as the analytical one calculated with Eq.(19), since the known displacement $(\Delta x, \Delta y)$ corresponds to the sub-pixel peak position (x_e, y_e) . For every displacement vector, the mean, maximum, minimum and the standard deviation of the sub-pixel displacement estimation error $\|\mathbf{d}_r^{sim}\|$ for different rotation angles and center positions was calculated. Using real data, the rotation angle and the center position of the particles is normally unknown, therefore the maximum can be used as a conservative estimate of the sub-pixel displacement estimation error.

The result of the simulation using elliptical particle images with an eccentricity of $\varepsilon = 0.866$ is displayed in Fig. 7–9 as a contour plot. Note that the one-dimensional Gaussian algorithm (see Fig. 7) using 3 values according to Eq. (3) provides nearly the same result as the one-dimensional Blais-Riou method (see Fig. 8) with a filter length of 5 (see Eq. (4)–(5)). The maximum error is about 0.4 pixel in both cases, but the minimum error when applying the Blais-Riou algorithm is much higher. This is due to the non-exact linear interpolation used by the Blais-Riou method whereas the minimum error of the Gaussian algorithm is very low, because the model used for the fit is the same as for gener-

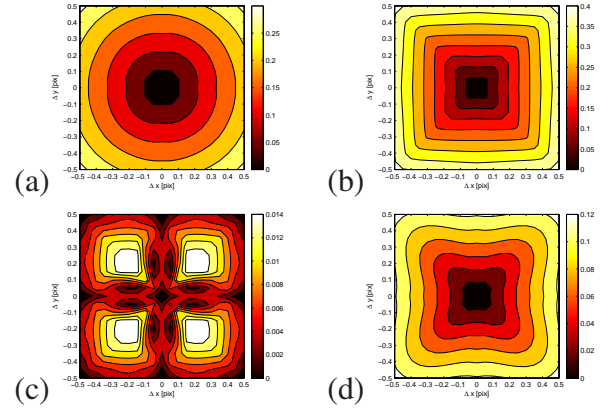


Fig. 8 Sub-pixel displacement estimation error using the one-dimensional Blais-Riou algorithm: (a) mean, (b) maximum, (c) minimum, (d) standard deviation.

ating the synthetic images. Hence, even the maximum error of the two-dimensional Gaussian algorithm (see Fig. 9(b)) using 9 values in a 3×3 area is in the order of computational accuracy.

In Tab. 1, a comparison of the maximum pixel errors of the numerical experiment with the analytical solution from Eq. (19) is provided for different eccentricities ε and known displacement $(\Delta x, \Delta y)$ (corresponding to a peak center position (x_e, y_e)). The maximum pixel errors of the one-dimensional algorithms (Blais-Riou and Gaussian algorithm) match very well the analytical description of the one-dimensional elliptical sub-pixel displacement estimation error $\|\mathbf{d}_r^{ana}\|$. The differences between the analytical equation and the numerical experiment are in the order of magnitude of 0.01 pixel for the Blais-Riou algorithm and 0.002 pixel for the Gaussian algorithm, respectively. As already noticed, the error increases for higher eccentricities ε and can reach nearly one pixel for $\varepsilon = 0.9682$.

To further verify the results given in Fig. 7–8 and Tab. 1, the simulated elliptically shaped particle images are evaluated with two commercial PIV evaluation software packages (see Tab. 2). These software packages (denoted by † and ‡ respectively) were tested extensively during the PIV challenge 2 (see [29]), where they performed better than most of their competitors. Both pack-

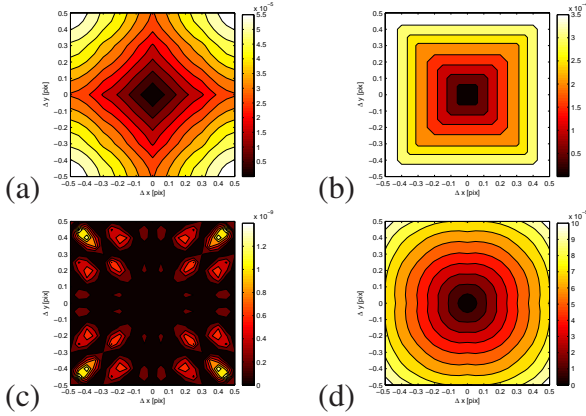


Fig. 9 Sub-pixel displacement estimation error using the two-dimensional Gaussian algorithm: (a) mean, (b) maximum, (c) minimum, (d) standard deviation.

ages provide the one-dimensional Gaussian algorithm (as a three-point operator), whereas package ‡ seems to be in quite good accordance to the analytical error. The software package † tends to over-estimate the bias error in case of $\epsilon = 0.7454$, but for $\epsilon = 0.9682$ the error is smaller the analytical one. For using the one-dimensional Gaussian algorithm with both packages, the bias error clearly exceeds the expected accuracy of 0.1 to 0.05 pixel given by [10]. The best result overall with the commercial PIV evaluation software packages is achieved by using the centroid operator with a kernel size of 9×9 pixel. The error of the centroid operator is always smaller than 0.05 pixel. The good result obtained by means of the centroid algorithm is due to the fact that all values inside the two-dimensional interrogation kernel are used to estimate the sub-pixel peak position and thus this operator is capable to handle with arbitrarily rotated elliptically shaped correlation peaks.

In Tab. 3 a comparison of the two-dimensional linear Gaussian algorithm introduced in section 2.2.1 and the two-dimensional non-linear iterative Levenberg-Marquardt algorithm using correlation values weighted according to the Fisher transform introduced by [26] is given. Both algorithms are able to handle elliptical correlation peaks without any signifi-

Table 1 Overview of the maximum pixel errors in elliptical sub-pixel displacement estimation using one-dimensional algorithms.

x_e	y_e	ϵ	1D Blais-Rioux	1D Gaussian	Analytical error (1D) $\max_{\alpha}(\ \mathbf{d}_r^{ana}\)$
0.25	0.0	0.7454	0.1068	0.1041	0.104
0.25	0.25	0.7454	0.1307	0.136	0.1358
0.5	0.5	0.7454	0.2672	0.272	0.2716
0.25	0.0	0.866	0.1958	0.1873	0.1875
0.25	0.25	0.866	0.2016	0.2125	0.2125
0.5	0.5	0.866	0.4112	0.425	0.425
0.25	0.0	0.9428	0.3363	0.3328	0.334
0.25	0.25	0.9428	0.3416	0.3415	0.3423
0.5	0.5	0.9428	0.6851	0.683	0.6846
0.25	0.0	0.9682	0.4682	0.4675	0.4667
0.25	0.25	0.9682	0.4729	0.4717	0.4705
0.5	0.5	0.9682	0.9433	0.9435	0.9409

Table 2 Comparison of the sub-pixel displacement estimation errors (in pixel) of different algorithms provided by two commercial PIV evaluation software packages denoted by † and ‡ respectively. The simulated image shift was $(\Delta x, \Delta y) = (0.5, 0.5)$ pixel.

ϵ	α	Centroid†	1D Gaussian†	1D Gaussian‡	Analytical error $\ \mathbf{d}_r^{ana}\ $
0.7454	10°	0.0357	0.35	0.1635	0.1138
0.7454	20°	0.033	0.3813	0.2203	0.1996
0.7454	45°	0.0247	0.4154	0.3442	0.272
0.8660	10°	0.032	0.4019	0.3025	0.2442
0.8660	20°	0.0413	0.46	0.4371	0.3805
0.8660	45°	0.0309	0.4965	0.4951	0.4243
0.9428	10°	0.0441	0.523	0.5774	0.5566
0.9428	20°	0.0518	0.6065	0.7182	0.683
0.9428	45°	0.0276	0.5817	0.5886	0.5657

Table 3 Comparison of the sub-pixel displacement estimation errors (in pixel) of two-dimensional Gaussian algorithms. The simulated image shift was $(\Delta x, \Delta y) = (0.5, 0.5)$ pixel.

ϵ	α	2D Gaussian (see section 2.2.1)	2D iterative Gaussian (see [26])	Analytical error (1D) $\ \mathbf{d}_r^{ana}\ $
0.7454	10°	0.0121	0.019	0.1138
0.7454	20°	0.01	0.0082	0.1996
0.7454	45°	0.0018	0.0093	0.272
0.8660	10°	0.0153	0.0222	0.2442
0.8660	20°	0.0114	0.0263	0.3805
0.8660	45°	0.0008	0.0043	0.4243
0.9428	10°	0.0133	0.0084	0.5566
0.9428	20°	0.011	0.0066	0.683
0.9428	45°	0.0021	0.0392	0.5657

cant bias error. Using the linear Gaussian algorithm from section 2.2.1, the maximum sub-pixel displacement estimation error in case of arbitrarily rotated elliptical particles is always smaller than 0.015 pixel. For the non-linear iterative Levenberg-Marquardt algorithm, the error is smaller than 0.04 pixel. The bias error of both algorithms are always smaller as the expected accuracy of 0.1 to 0.05 pixel given by [10] and should, therefore, be used in any application of cross-correlation based measurement techniques in aerodynamics where elliptically shaped correlation peaks can occur instead of the most commonly used one-dimensional three-point estimators.

5 Summary and conclusions

Using one-dimensional sub-pixel displacement estimation algorithms in each coordinate direction will introduce a bias error in the estimated two-dimensional displacement in case of arbitrarily rotated elliptically shaped correlation peaks. An analytical equation of this bias error was therefore derived. It depends on the center position (x_e, y_e) , the eccentricity ε and the rotation angle α of the ellipse and can lead to a systematic influence of more than one pixel. A gradient-based algorithm for sub-pixel displacement estimation, the so-called Blais-Rioux method, which was originally developed for application in laser triangulation, was applied to cross-correlation based measurement techniques. This approach does not use a priori information about the shape of the correlation peak. To avoid bias errors in sub-pixel displacement estimation of elliptically shaped correlation functions, a general linear two-dimensional Gaussian algorithm was presented, which has a systematic error (in case of arbitrarily rotated elliptical particles) always smaller than 0.015 pixel. It should be noted that two-dimensional algorithms assuming a circular shaped correlation peak will lead to the same result as one-dimensional algorithms in case of arbitrarily rotated elliptical peaks. Hence, the presented general two-dimensional linear Gaussian algorithm should be implemented in commercial

software packages for data evaluation in experimental aerodynamics because it is very accurate and easy to implement. Future research could be the investigation of gradient-based algorithms on a two-dimensional domain and the investigation of the robustness of Gaussian algorithms in the presence of noise.

References

- [1] Förstner W. On the geometric precision of digital correlation. *Int. Archives of Photogrammetry and Remote Sensing (IAPRS)*, Vol. 24, No. 3, pp 176-189, 1982.
- [2] Ackermann F. High precision digital image correlation. *Proc. 39th Photogrammetrische Woche*, Stuttgart, Germany, 1983.
- [3] Ackermann F. Digital image correlation: performance and potential applications in photogrammetry. *Thompson Symp.*, Birmingham, U.K., 1984.
- [4] Grün A. Adaptive least squares correlation: a powerful image matching technique. *South African Journal of Photogrammetry, Remote Sensing and Cartography*, Vol. 14, pp 175-187, 1985.
- [5] Peters W H and Ranson W F. Digital imaging techniques in experimental stress analysis. *Opt. Eng.*, Vol. 21, pp 427-431, 1982.
- [6] Siebert T, Becker T, Spiltthof T, Neumann I and Krupka R. High-speed digital image correlation: error estimations and applications. *Opt. Eng.*, Vol. 46, No. 051004, pp 1-7, 2007.
- [7] Willert C and Gharib M. Digital particle image velocimetry. *Exp. Fluids*, Vol. 10, pp 181-193, 1991.
- [8] Westerweel J. Fundamentals of digital particle image velocimetry. *Meas. Sci. Technol.*, Vol. 8, Special Issue on Particle Image Velocimetry, pp 1379-1392, 1997.
- [9] Scarano F. Iterative image deformation methods in PIV. *Meas. Sci. Technol.*, Vol. 13, pp R1-R19, 2002.
- [10] Raffel M, Willert C, Werely S T and Kompenhans J. *Particle Image Velocimetry: A Practical Guide*. 2nd edition, Springer, 2007.
- [11] Konrath R, Klinge F, Schröder A, Kompenhans J and Füllekrug U. The projected pattern cor-

- relation technique for vibration measurements. *6th Int. Conf. on Vibration Measurements by Laser Techniques*, Ancona, Italy, 2004.
- [12] Blumrich F, Schröder A, Konrath R and Klinge F. Presentation of two optical correlation-based measurement techniques for surface deformation: PROPAC and REPAC. *Proc. SENSOR Conference 2007*, Nuremberg, Germany, Vol. 2, pp 117-123, 2007.
- [13] Richard H and Raffel M. Principle and applications of the background oriented schlieren (BOS) method. *Meas. Sci. Technol.*, Vol. 12, pp 1576-1585, 2001.
- [14] Kindler K, Goldhahn E, Leopold F and Raffel M. Recent developments in background oriented Schlieren methods for rotor blade tip vortex measurements. *Exp. Fluids*, Vol. 43, pp 233-240, 2007.
- [15] Bing P, Hui-min X, Bo-qin P and Fu-long D. Performance of sub-pixel registration algorithms in digital image correlation. *Meas. Sci. Technol.*, vol. 17, pp 1615-1621, 2006.
- [16] Chen J and Katz J. Elimination of peak-locking error in PIV analysis using the correlation mapping method. *Meas. Sci. Technol.*, Vol. 16, pp 1605-1618, 2005.
- [17] Fisher R B and Naidu D K. A comparison of algorithms for subpixel peak detection. Sanz J. (Eds.), *Image Technology, Advances in Image Processing, Multimedia and Machine Vision*, Springer, pp 385-404, 1996.
- [18] Trucco E, Fisher R B, Fitzgibbon A W and Naidu D K. Calibration, data consistency and model acquisition with a 3-d laser striper. *Int. J. of Computer Integrated Manufacturing*, Vol. 11, pp 292-310, 1998.
- [19] Blais F and Rioux M.. Real-time numerical peak detector. *Signal Processing*, Vol 11, pp 145-155, 1986.
- [20] Gühring J. *3D-Erfassung und Objektrekonstruktion mittels Streifenprojektion*. PhD thesis, University of Stuttgart, 2002.
- [21] Whittaker E T. On the functions which are represented by the expansions of the interpolation theory. *Proc. Roy. Soc.*, Vol. 35, pp 181-194, 1915.
- [22] Roesgen T. Optimal subpixel interpolation in particle image velocimetry. *Exp. Fluids*, vol. 35, pp 252-256, 2003.
- [23] Alexander B F and Ng K C. Elimination of systematic error in subpixel accuracy centroid estimation. *Opt. Eng.*, Vol. 30, pp 1320-1331, 1991.
- [24] Condon J J. Errors in elliptical gaussian fits. *Astronomical Society of the Pacific*, Vol. 109, pp 166-172, 1997.
- [25] Nobach H and Honkanen M. Two-dimensional gaussian regression for sub-pixel displacement estimation in particle image velocimetry or particle position estimation in particle tracking velocimetry. *Exp. Fluids*, Vol. 38, pp 511-515, 2005.
- [26] Ronneberger O, Raffel M and Kompenhans J. Advanced evaluation algorithms for standard and dual plane particle image velocimetry, *Proc. 9th Int. Symp. on Applications of Laser Techniques to Fluid Mechanics*, Lisbon, Portugal, 1998.
- [27] Davis C Q and Freemann D M. Statistics of subpixel registration algorithms based on spatiotemporal gradients or block matching. *Opt. Eng.*, Vol. 37, pp 1290-1298, 1997.
- [28] Schreier H W, Braasch J R and Suttton M A. Systematic errors in digital image correlation caused by intensity interpolation. *Opt. Eng.*, Vol. 39, pp 2919-2921, 2000.
- [29] Stanislas M, Okamoto K, Kähler C J and Westerweel J. Main results of the second international PIV challenge. *Exp. Fluids*, Vol. 39, pp 170-191, 2005.

5.1 Copyright Statement

The authors confirm that they, and/or their company or organization, hold copyright on all of the original material included in this paper. The authors also confirm that they have obtained permission, from the copyright holder of any third party material included in this paper, to publish it as part of their paper. The authors confirm that they give permission, or have obtained permission from the copyright holder of this paper, for the publication and distribution of this paper as part of the ICAS2010 proceedings or as individual off-prints from the proceedings.